

Shape reconstructions and morphing kinematics of an eagle during perching manoeuvres*

Di Tang(唐迪)^{1,2,†}, Dawei Liu(刘大伟)², Hai Zhu(朱海)¹, Xipeng Huang(黄喜鹏)¹,
Zhongyong Fan(范忠勇)³, and Mingxia Lei(雷鸣霞)³

¹College of Mechanical Engineering, Zhejiang University of Technology, Hangzhou 310014, China

²High Speed Aerodynamic Institute, China Aerodynamics Research and Development Center, Mianyang 621000, China

³Zhejiang Museum of Natural History, Hangzhou 310014, China

(Received 21 August 2019; revised manuscript received 18 November 2019; accepted manuscript online 12 December 2019)

The key to high manoeuvre ability in bird flight lies in the combined morphing of wings and tail. The perching of a wild *Haliaeetus Albicilla* without running or wing flapping is recorded and investigated using a high-speed digital video. A shape reconstruction method is proposed to describe wing contours and tail contours during perching. The avian airfoil geometries of the *Aquila Chrysaetos* are extracted from noncontact surface measurements using a ROMBER 3D laser scanner. The wing planform, chord distribution and twist distribution are fitted in convenient analytical expressions to obtain a 3D wing geometry. A three-jointed arm model is proposed to associate with the 3D wing geometry, while a one-joint arm model is proposed to describe the kinematics of tail. Therefore, a 3D bird model is established. The perching sequences of the wild eagle are recaptured and regenerated with the proposed 3D bird model. A quasi-steady aerodynamic model is applied in the aerodynamic predictions, a four-step Adams–Bashforth method is used to calculate the ordinary differential equations, thus a BFGS based optimization method is established to predict the perching motions.

Keywords: large bird of prey, shape reconstruction, morphing kinematic, perching

PACS: 47.32.cd, 47.32.Ff

DOI: 10.1088/1674-1056/ab610a

1. Introduction

A flying animal flaps its wings to generate both thrusts and lifts to balance the drag and weight. After thousands of years of evolution, the wing of flying animals moves generally with complex patterns in both wing kinematics and deformations,^[1] and a bird can colonize almost all terrestrial habitats on earth, such as cliff, distant islands. Different flying animals have different flight features, resulting in various aerodynamic mechanisms. For example, a fruit fly beats its wings with a very high frequency (about 100 Hz) to generate lift as higher as possible. The main feature is the strong unsteady flow with a low Reynolds number which restricts its thrust generations and high lifts.^[2–4] Unlike the insect, a bat usually flies at a speed of 3–5 m/s, and the flapping frequency is about 10 Hz during a moderate flight.^[5] On the other hand, characteristic speed of a pigeon is about 15 m/s, with wing flapping at a frequency of 1–2 Hz. The generated lift coefficient is about 0.47 and quasi-steady aerodynamics can be used to predict the lifts and drags.

A detailed learning of avian locomotion is an essential step in revealing the excellent flight abilities of bird flight.^[6] Unique flight form of wingbeats once intrigued scientists, recording the form of wingbeats has been a long issue.^[7,8] Measurements of bird flight were raised by Brown over 60 years ago, and then some theoretical models were proposed

to analyze aerodynamic mechanisms of bird flight.^[9–13] An inverse computational method originated from modelling terrestrial locomotion, which gives an opportunity to simulate wingbeats without inputting measured kinematic data.^[14,15] Recently, Parslew and Crowther proposed and validated a robust theoretical model for predicting the form of avian wingbeats using the inverse computational method.^[16] The avian wing geometry of large bird, such as seagull, merganser, teal and owl have also been investigated.^[17,18] Geometry shapes of a bird wing, including airfoils, can be quantified using analytical expressions, and a jointed arm model was also developed to represent the avian wing kinematics recovered from videos. The primary feather has important effects on the aerodynamics, the cutting of primary feathers at the tip will reduce the distance flown dramatically.^[19] Recently, we proposed a modified 3D model of barbs to describe separating and recovering processes of neighboring barbs, the critical connecting force between barbs were quantified by an experimental approach.^[20] The airfoil in the position of 40% spanwise of the long-eared owl wing has excellent aerodynamic performance and low noise characteristics. It is studied and extracted to reconstruct the bionic blades with improved aerodynamic performances by Qu and Liu.^[21] It is impressive that the perching of steppe eagle *Haliaeetus Albicilla* was studied.^[22] The aeroelastic deflections of the covert feathers of an eagle

*Project supported by the National Natural Science Foundation of China (Grant No. 51705459) and the China Postdoctoral Science Foundation.

†Corresponding author. E-mail: tangdi@zjut.edu.cn

were investigated using onboard and high-speed digital video during wide-ranging free flight. Also, high-resolution and high-speed digital videos were used to study indoor and outdoor perching manoeuvres.^[23,34] It has been raised that rapid pitch-up plays an important role in high manoeuvrability of a large prey which enables the bird to speed down, change direction or climb in a short time. During the rapid pitch-up, kinetic energy was changed to potential energy. Lift can be enlarged incredibly under a large angle of attack of the up stroking, which will drive a bird upward. As the deep stall, the drag can be enlarged to induce the loss of the total kinetic energy to the wake.^[25] Both the high lift and the high drag offer the opportunity to change the flight attitude quickly.

After investigations of hundreds of flying videos of large birds of prey, such as gliding, hovering, perching, and fighting, it is the combined morphing of wing and tail that allow an eagle change its flight attitude in the shortest time (flapping is unnecessary). Also, rapid transition between a steady glide and a deep stall often appears.^[23] During those maneuvering flights, perching with zero running distance is one of the most simple but basic flight patterns. An eagle was observed to land on the ground without running or wing flapping but with combined morphing of wing and tail to achieve a “soft landing”. The corresponding perching sequences were investigated. A bird skin construction method was also proposed to describe motions of both wing and tail, the perching sequences of the eagle was also numerically reproduced.

2. Specimen and experiment

2.1. Specimen of *Aquila Chrysaetos*

Aquila Chrysaetos is a large bird of prey, and it has quite excellent flying abilities, which help it perching and fighting, etc. However, the *Aquila Chrysaetos* is a first-class national protected animal of China, any sale, purchase or use of the wild animal or its products is forbidden.

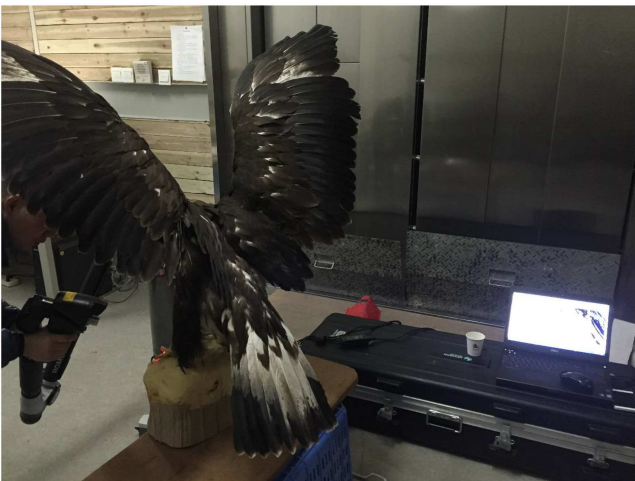


Fig. 1. Three-dimensional scanning scene and specimen of the eagle.

The scanning object is a specimen of *Aquila Chrysaetos* at Zhejiang Museum of Natural History as shown in Fig. 1. The *Aquila Chrysaetos* was processed at a flying posture and the specimen has been well kept. Before the scanning, a kind of alcohol for specimen was used to clear each feather of the wing and the tail. Also, each feather was repaired and rearranged to ensure the exact flying shape.

2.2. Three-dimensional scanning of wing and tail

We used a ROMBER absolute arm with integrated scanner to which a three-dimensional non-contact laser scanner is attached for the bird surface measurements. The ROMBER absolute arm is a hand-held mechanical device with high accuracy. Before the experiment, the ROMBER arm was fixed to the ground using glue to ensure that the tower of the ROMBER will keep unmoved. On the ROMBER arm, the position of the scanner relative to a given coordinate system is known accurately. An integrated laser scanner is designed to capture 3D point data across a range of surface types. With an ultra-wide laser stripe of up to 150 mm, the scanner can capture 7520000 points per second. The accuracy of the complete scanning system is verifiable and traceable, the accuracy of surface data is within 0.01 mm. Operating with the Geomagic Wrap software, the system works based on the principle of laser stripe triangulation. A laser line was project onto the object and the line was viewed by cameras so that distance variations on the object can be seen. The resulting scanning data will be a profile that contains the shape information. The scanner can work for a variety of materials and colors including black and white which are common for the feathers of *Aquila Chrysaetos*. The Geomagic Wrap software can output data in a CATIA format, which be dealt using the data cloud method.

Figure 2 shows the obtained point cloud with wing, tail and flight feathers identified in sequence. Each section cut through a flight feather shaft represents a combined airfoil with both a traditional airfoil (part 1) and a flight feather (part 2) assembled, as shown in Fig. 2(c). The corresponding secondary flight feather is shown in Fig. 2(d). The primary flight feather plays an important role in flights. However, it has different shape compared with the secondary one. No reports about flight feather shape was observed yet, thus the width of the feather along the rachis was marked to quantify the feather shape as shown in Fig. 2(e).

The scanned tail point cloud is shown in Fig. 2(f), and 12 tail feathers were identified in sequence. The thickness of the tail feather is so small that can be ignored regarding the large length of the feather. Each tail feather was simplified to a rigid body, thus leading edge, left side and right side were indicated to illustrate the tail contours.

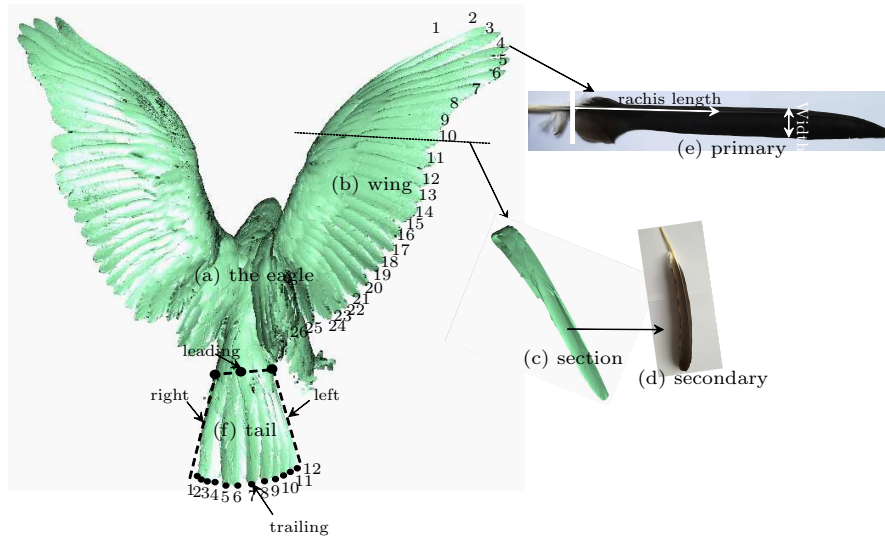


Fig. 2. Sketch of the eagle with identifications of wing and tail: (a) point cloud of the eagle, (b) wing with identification of 26 flight feathers, (c) a section of the scanned point cloud, (d) the scanned secondary flight feather, (e) the scanned primary feather with instructions of rachis and feather width, (f) the tail with identification of 12 tail feathers.

3. Airfoil modeling and shape construction

The wing is covered with covert feathers and flight feathers, the coverts provide most of the lower surface contour and all the upper surface contour over the thick forward sections. The under-wing and upper-wing once were anatomical identified as seven regions.^[26] To the simplify the wing shapes, the sectional airfoil cut through a primary feather is decomposed into two parts. They are named as part 1 and part 2, which are a typical wing airfoil (without primary feather) and a primary feather respectively, as shown in Fig. 3. The main motivation for this classification is that the primary feather may move or rotate relative to part 1, also some empirical functions have been summarized for the typical airfoil of part 1 and can be conveniently adopted here.^[17,27]

As part 1, the camber line and the thickness distribution were quantified first, thus the upper surface was expressed as an addition of the camber line and thickness distribution, the lower surface was expressed as a subtraction of the camber line and thickness distribution,

$$z_{upper} = z_{(c)} + z_{(t)}, \quad (1)$$

$$z_{lower} = z_{(c)} - z_{(t)}. \quad (2)$$

To quantify the mean camber line from wing surface measurements, the Birnbaum–Glauert camber line was used,^[24]

$$\frac{z_{(c)}}{c} = \frac{z_{(c)\max}}{c} \eta (1 - \eta) \sum_{n=1}^3 S_n (2\eta - 1)^{n-1}, \quad (3)$$

where $\eta = x/c$ is the normalized chordwise coordinate, $z_{(c)\max}$ is the maximum camber coordinate, c is the local wing chord length. The thickness distribution is quantified as

$$\frac{z_{(t)}}{c} = \frac{z_{(t)\max}}{c} \sum_{n=1}^5 A_n (\eta^{n+1} - \sqrt{\eta}), \quad (4)$$

where $z_{(t)\max}$ is the maximum thickness, coefficients A_n are to be determined. The maximum order 6 was used here.

As part 2, a local coordinate was arranged at the feather root, an exponential function was used to describe the bending of the secondary feather along the x axis,

$$\frac{\omega_{(t)}}{c} = \frac{\omega_{(t)\max}}{c} \phi e^{\psi}, \quad (5)$$

where $w_{(t)\max}$ is the maximum bending at the tip of the secondary feather.

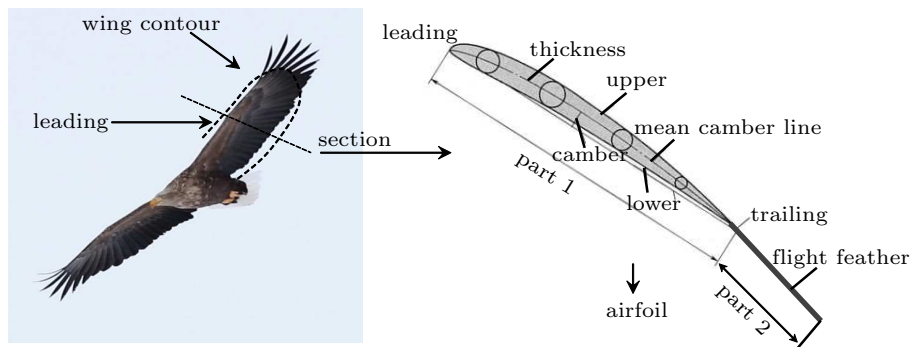


Fig. 3. Illustration of wing contour and the simplified airfoil with a flight feather.

Since the particular length of part 1 and part 2 of each feather can be obtained, the chord distributions along the span were obtained by measuring the 26 airfoils. The wing planform was also measured by locating leading points and trailing points along the span. Each tail feather is assumed to have the same length distribution and width distribution, which was assembled to be a cylindroid body. Thus, a fan-shape tail was expected for the eagle and no thickness of tail feather was considered in the current research.^[28]

4. Method for predicting kinetics of the eagle

4.1. Bones and simplified arms

The bird wing skeleton consists of the humerus which is attached to the muscles in the breast, ulna, radius, carpometacarpus and phalanges,^[29] as shown in Fig. 4. The humerus was simplified to one shoulder arm, both the radius and the ulna were simplified as one elbow arm, the carpometacarpus was simplified to one wrist arm, as shown in Fig. 5. One shoulder joint was used to connect the proximal shoulder arm with the body, one elbow joint was used to connect the distal shoulder arm with the proximal elbow arm, while the distal elbow arm was connected with the proximal wrist arm using a wrist joint. On the other hand, only small deformations of tail feather were observed, thus a tail feather can be simplified to a rigid one during flight. The left tail feather and the right feather were identified as a left tail arm and a right arm, respectively. All the other tail feathers equally distributed between the two arms, which were connected to the tail with joints. As an approximate wing and tail model, the multiple-jointed rigid arm system was used to determine the kinematics of the eagle.^[29]

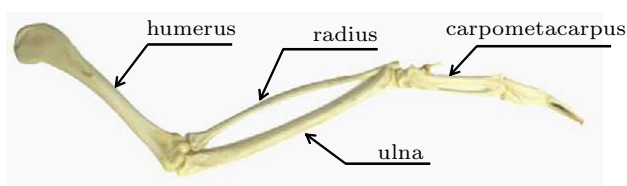


Fig. 4. Photograph of the bones in the left wing of a turkey vulture.^[30]

The skeleton structure was described as a three-jointed arm system along the quarter-chord line of a wing. The orientation of each arm can be changed by pitching the trunk and rotating around the corresponding joint.^[31] As shown in Fig. 6(a), the shoulder arm rotates around point O_1 in a body coordinate system (illustrated in Fig. 5), where the origin O_1 locates at the wing root. The planes XO_1Y and YO_1Z are defined as rotational planes of the shoulder arm which can also rotate around its bone axis. Thus, the shoulder arm moves with three degrees of freedom defined by the Euler angles ϕ_1 , ψ_1 and ω_1 .^[32] In contrast, only the plane YO_2Z is defined as

the rotational plane of the elbow arm which can also rotate around its axis. Thus, the motion of elbow arm has two degrees of freedom defined as ψ_2 and ω_2 . The wrist arm moves with two degrees of freedom, which are given by the angles ϕ_3 and ψ_3 . This three-jointed arm model with seven degrees of freedom allows the recovery of the morphing kinematics of a wing precisely, it can also serve as a straightforward model for analyzing a mechanical wing.

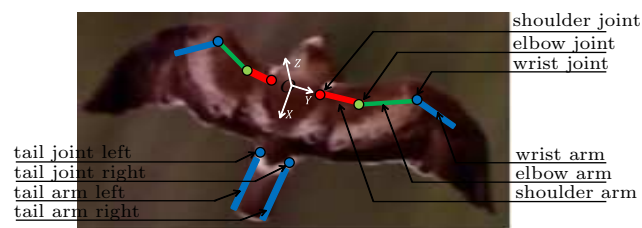


Fig. 5. A sketch of simplified arms and joints on the photo of an eagle photographed in Thousand-Island Lake, Hangzhou.

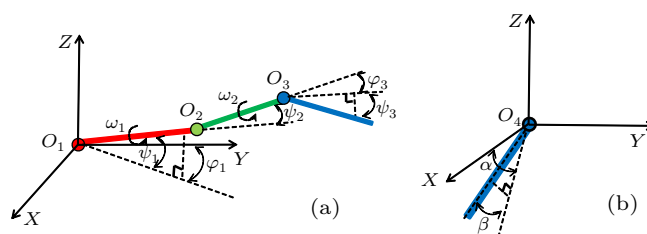


Fig. 6. Simplified skeleton structures of an eagle: (a) wing, (b) tail.

Another simple skeleton structure was described as a one-jointed arm system to represent the border line of the tail, although no skeleton exists in tail feathers. Take the right tail arm as an example as shown in Fig. 6(b), it rotates around a point O_4 in a body coordinate system, where the origin O_4 locates in the tail. The plane XO_4Y and XO_4Z are defined as the rotational planes of the tail arm. Thus, the motion of tail arm has two degrees of freedom defined as α , β . With the cooperations of left tail arm and right tail arm, typical motions of tail, such as downward/upward, antisymmetric twist, swing side to side, can be reconstructed.

4.2. Kinematics equations of arms

Each bone of a bird was treated as a rigid body connected by the corresponding joint, whereas the skin was flexible with morphing abilities.^[33] The position and kinematics of the quarter-chord line of a wing to a fixed body coordinate system was described by a simplified arm, the arm motions were represented by the motion of floating frame of reference.^[34] The total generalized coordinates of the i -th rigid body is $q_i = [x_i, y_i, z_i, \phi_i, \theta_i, \psi_i]^T$, where $[x_i, y_i, z_i]^T$ are locations of a body, $[\phi_i, \theta_i, \psi_i]^T$ are Euler angles.^[34] When a body moves with both rotations and translations, a point P location of body i can be written as

$$r_i = r_{i0} + A_i u_{i0}, \quad (6)$$

where r_{i0} is the location of i -th body center under the global Cartesian coordinate, A_i is the Euler rotation matrix of the floating frame, u_{i0} is the location under the floating frame. Velocity and acceleration at the point P can be obtained by differentiating Eq. (2):

$$\dot{r}_i = \dot{r}_{i0} + \dot{A}_i u_{i0}, \quad (7)$$

$$\ddot{r}_i = \ddot{r}_{i0} + \ddot{A}_i u_{i0}. \quad (8)$$

4.3. Kinetics and aerodynamics modelling

A 2D flight was assumed in the perpendicular plane, the equations of motion of an eagle were given in the ground coordinate system as follows:

$$m\ddot{x} = D, \quad (9)$$

$$m\ddot{y} = L - mg, \quad (10)$$

where F_x and F_y are the aerodynamic drag and lift arising from dynamic motion of wings; m is the total mass; g is the acceleration of gravity; x and y are locations in the x -direction and z -direction, respectively. It should be noted that no flapping was observed during the perching, thus the thrust was not accounted in the current research. The aerodynamic drag and lift acting on the trunk were given as^[35,36]

$$D = \frac{1}{2} \rho v_\infty^2 s c_d, \quad (11)$$

$$L = \frac{1}{2} \rho v_\infty^2 s c_l, \quad (12)$$

where ρ is the air density, s is the wing area, c_d and c_l are the drag coefficient and lift coefficient respectively. Since the quasi-steady aerodynamic models have been successfully applied in the aerodynamic prediction, the aerodynamic force coefficients were modeled as trigonometric functions of angle of attack, which are independent of airfoil geometry.^[37] The flight feathers have important effects on the aerodynamics, ignores of primary feathers at the tip will reduce the distance flown dramatically.^[19] To considerate these flight feather effects, the enhancement of lifts and increasement of wing area s are included in Eqs. (11) and (12) based on the previous researches,^[25]

$$c_d = B + C \cos(2\alpha), \quad (13)$$

$$c_l = A \sin(2\alpha). \quad (14)$$

Here a value of $A = 1.64$, which defines the maximum aerodynamic lift coefficient, was used based on the experimental data of Usherwood. Values of $B = 1.135$ and $C = -1.05$ once were assumed to be appropriate for an arbitrary airfoil.^[16,38] However, the drag reduction rate of feather-like surface was experimentally proved to be about 16% than traditional microgroove riblet.^[39] Thus, more smaller drag coefficient was used by setting $C = -1.1$.

5. Method for shape regeneration

5.1. Capturing video and shape regeneration

To capture the perching sequences, the flying video was recorded with high-speed camera with the help of Zhejiang Museum of Natural History, as shown in Fig. 7. Before photographing, some fish and meat were used to attract the Aquila Chrysaetos, since then our professional photographers were kept away from the right place. An approach was used to deal with the recorded video frame: each frame in the video was extracted with the Matlab software by the function of VideoReader, as shown in Fig. 8. The motions of wing and tail were quantified with freedoms of multi-body systems $q_i = [x_i, y_i, z_i, \phi_i, \theta_i, \psi_i]^T$. How the bones behaved against time were reconstructed with the freedoms of the multi-body system,^[40] followed by the reconstruction of bird shape with the coupling approach discussed in Section 2. The reconstructed shape was also compared with the recorded video to ensure that the motion of birds was captured precisely. Thus, how the bird flies during deep stall was reproduced with the obtained control strategy.

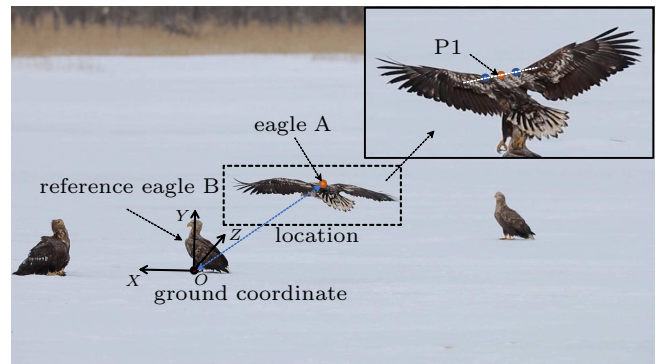


Fig. 7. An approach for reconstructing bird shapes during perching.

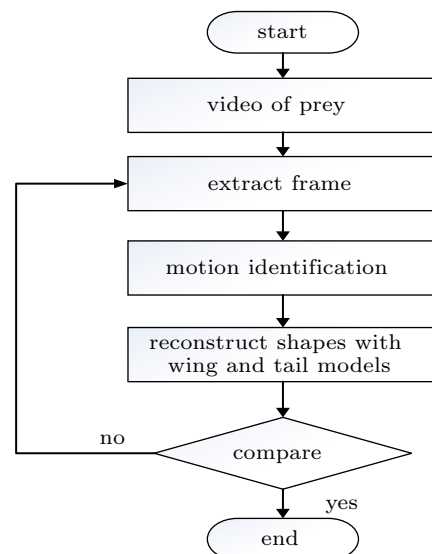


Fig. 8. An approach for reconstructing bird shapes during perching.

It is lucky that an eagle B was still kept during the whole perching of eagle A. thus, it is convenient to locate a ground coordinate system at the foot of eagle B, as shown in Fig. 7. The center point of the two shoulders was monitored as P1 to represent the bird-A motion. Each frame was extracted, and the location of eagle A can be estimated by comparing the relative distance of the eagle A to the eagle B. Therefore, the motion of eagle A was established.

5.2. A method for predicting the control strategy during perching

To predict the eagle motions during perching, unsteady aerodynamics at each time step was calculated by the method described in Subsection 4.3. It should be noted that both the induced velocity and the eagle motion velocity were deducted to get the effective angle of attack which was thereafter applied to calculate the aerodynamic loads.^[16] The eagle motion was calculated by solving an ordinary differential equation (ODE) with a four-step Adams–Bashforth method which was detailedly described in Ref. [13].

where $L_{x,Pre}$ and $L_{y,Pre}$ are predicted displacements, $L_{x,Exp}$ and $L_{y,Exp}$ are experimental displacements.

6. Results and discussion

6.1. Airfoils and bird shape reconstruction

Equations (1)–(5) were defined as user defined functions in the Matlab software, then a curving fitting method was used to extract the coefficients S_n, A_n, ϕ, ψ for the camber line, thickness line and trail line from measurements of the eagle wing. Those fitting coefficients are listed in Table 1, and the interpolated normalized wing planform, chord distribution, twist distribution and tail line were generated with these coefficients, which are compared in Fig. 10. It is indicated that the measured data present a statistical property pointed by Riegels, as described by us in Ref. [25], and the fitted curves match with the measured data well. The deviations of the fitting airfoil from the measurement points in terms of the local maximum values $z_{(c)max}, z_{(t)max}$ and $\omega_{(t)max}$.

Table 1. Coefficients for the bionic airfoil.

S_1	S_2	S_3	A_1	A_2	A_3	A_4	A_5
3.6	1.5	0.3	-4.8	66.2	-199.8	235.6	-97.6

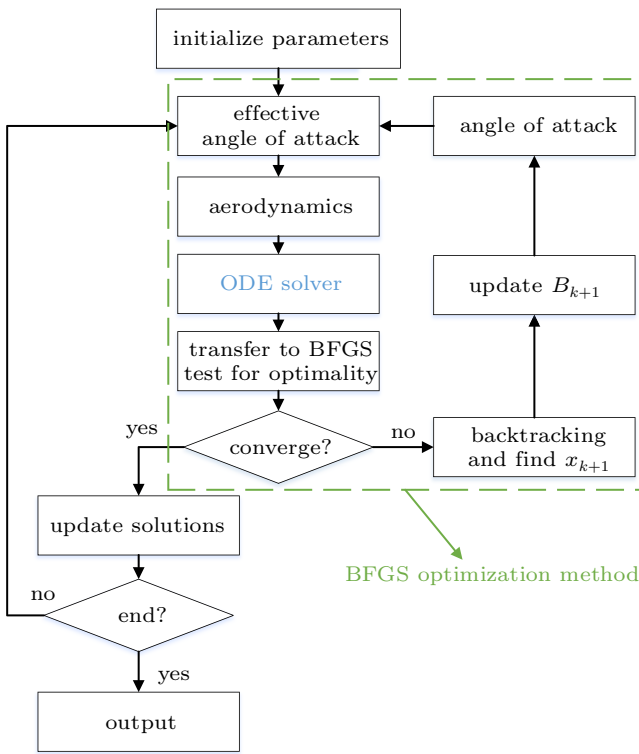


Fig. 9. An optimal approach for predicting the eagle motions.

A BFGS optimization method was used to reconstruct and predict the eagle motions by combining an objective function with the derivative-free line search method based on the approximate norm descent condition as shown in Fig. 9. The optimization method was a well-designed method and has been successfully used.^[34,41] The corresponding minimal function is defined as

$$\min F(x) = \sqrt{(L_{x,Pre} - L_{x,Exp})^2 + (L_{y,Pre} - L_{y,Exp})^2}, \quad (15)$$

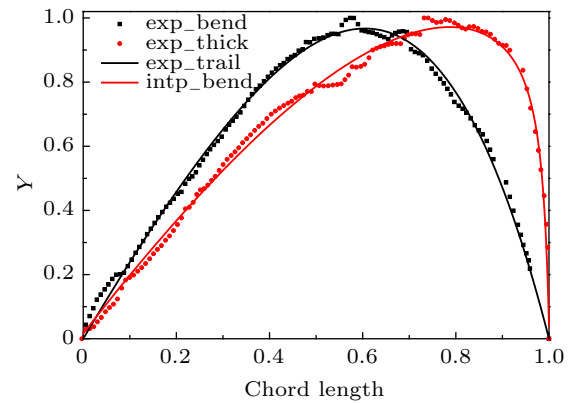


Fig. 10. Camber line and thickness distribution of the Aquila Chrysaetos.

An optimized width distribution of a flight feather was obtained with Gaussian functions as

$$f(x) = a_1 e^{-\left(\frac{x-b_1}{c_1}\right)^2} + a_2 e^{-\left(\frac{x-b_2}{c_2}\right)^2} + a_3 e^{-\left(\frac{x-b_3}{c_3}\right)^2}. \quad (16)$$

Table 2. Coefficients of flight feather.

a_1	b_1	c_1	a_2	b_2	c_2	a_3	b_3	c_3
0.917	0.002	0.001	0.667	0.012	0.004	0.605	0.006	0.004

Figure 11 displays the optimized width distribution of the primary feather, where the largest width was found at 11.2% station of the rachis. A flight feather grows in the wing muscle, and a feather root is always covered by coverts. Only the exposed flight feather length (part 2) was measured. Figure 12 displays the distribution of chord length along the span. The

last six primary feathers near wing tip have the longest length except the first one, while the four secondary feathers near wing root have the shortest length.

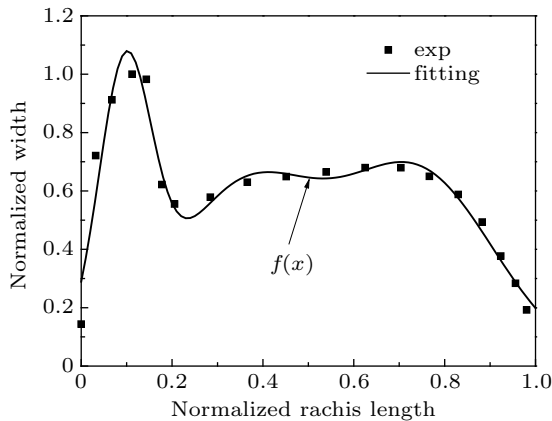


Fig. 11. Distribution of feather width along the rachis.

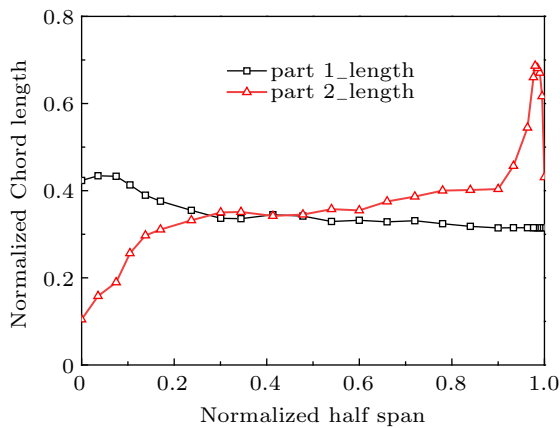


Fig. 12. Chord distributions along the span.

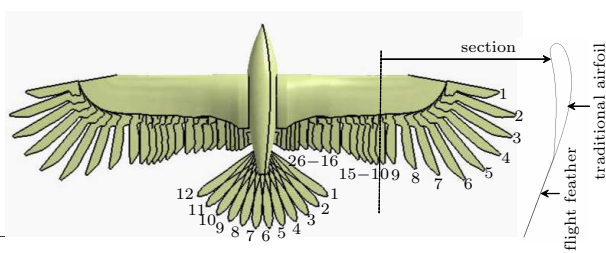


Fig. 13. Reconstructed eagle shape with 26 flight feathers, 12 tail feathers and a simplified body.

Figure 13 shows the reconstructed eagle shape with 26 flight feathers and 12 tail feathers. Considering that combined motions of both wings and tail play the most important role in aerodynamics during perching, both head and body of the bird were not the emphasis in the current study and they were simplified to a cylinder. A cross section was cut through the 10-th flight feather to show a typical *Aquila Chrysaetos* airfoil, where the airfoil with no primary feather is similar to the seagull or S1223 airfoil described by Liu.^[17] The flight feather was assembled to the traditional airfoil (part 1) according to the rule of curvature continuity at upper surface of the trailing edge.

6.2. Animals

A wild *Haliaeetus Albicilla* was chosen for the present flight study. Both the flying abilities and the somatypes of the *Haliaeetus Albicilla* compare favorably with those of the *Aquila Chrysaetos*. The bird mass was estimated to be 2.0 kg approximately as a matter of experience, and a span was estimated to be 2.0 m from left wingtip to wingtip which is close to the scanned *Aquila Chrysaetos*. The photography was taken with the help of Zhejiang Museum of Natural History. The recording was obviously not to pose any risk of causing pain, damage of harm to the wild animal involved.

6.3. Morphing of wing and tail during perching manoeuvres

The conventional design objectives or optimization objectives are usually the high lift-drag ratio. However, the key to the high manoeuvrability in bird flight lies not in the high lift-drag ratio or high lift performances, but in the way the wing morph to change the flying situations. Gliding, fighting, perching, and preying, etc. are the irrefutable proofs of this high manoeuvrability. Perching is one of the simplest wing motions with both the body attitude and flying attitude changed,^[25] and the perching motions of a *Haliaeetus Albicilla* was studied in the present study as shown in Fig. 14. Firstly, the *Haliaeetus Albicilla* glided to find the destination to rest with wing straightens before 0.0 s, followed by wing twists, tail spreads and pushes downwards at 2.0 s. When approaching its destination, it executed a rapid pitch-up before 4.0 s. During the flight, a pitching moment was generated to pitch the bird upwards rapidly. At the end of the rapid pitch-up at 4:00 s, the wing outstretched to give a parachute-like shape, wrist sweeps upward with large angle of attack to undergo deep stall. Before landing, tail began to shrink and pushed upwards to prevent strikes on the ground (actually, it was snow). Finally, it inhabited with claws touched the ground. During the flights, no flapping or running was observed, but rapid pitch-up. The claws touched the snow with a soft landing model. It is worth mentioning that this perching scene of the wild eagle is very rare, and a lot of time was spent for its appearance.

6.4. Bird motions during perching

The experimental (Exp), fitted (Fit), and predicted (Pre) eagle displacements and velocities (Exp) were compared and illustrated in Fig. 15 during perching. Displacements L_x was unified with 16.9 m and was fitted using a fourth-order polynomial $f(x)$, while the L_y was unified with 2.1 m and was fitted with $g(x)$. Coefficients of the two polynomials were listed in Table 3.

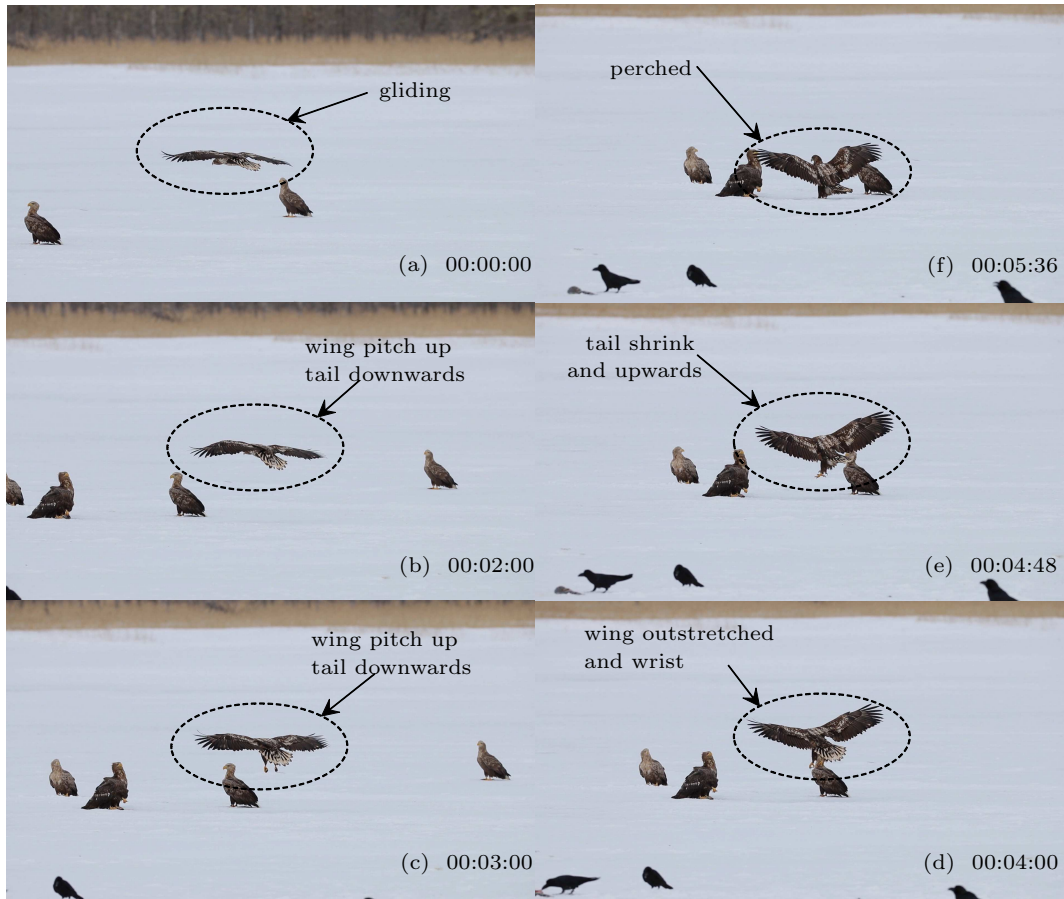


Fig. 14. Gliding perching sequence taken with high-speed digital video camera: (a) The eagle glides with wing straightens; tail spreads and flicked up and back. [(b), (c)] Wing twists, tail spreads and pushes downwards to endure rapid pitch-up. (d) Wing outstretched to give parachute-like shape and wrist swept upward to undergo deep stall. (e) Tail began to shrink and pushes upwards to prevent strikes. (f) Perched with zero running distance, and wrist sweeps forward.

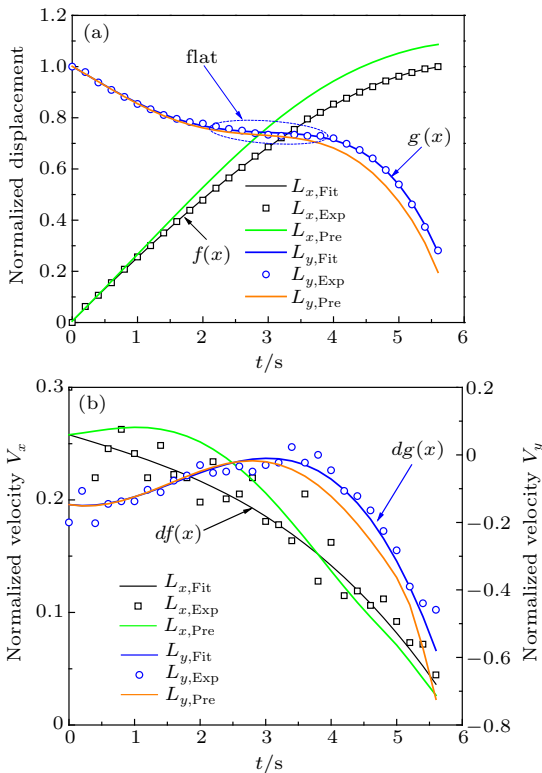


Fig. 15. Comparison of the eagle motions with the experimental method (Exp), fitting approach (Fit), and predicting method (Pre): (a) displacement, (b) velocity.

Table 3. Coefficients for the fitted polynomials.

p	p_1	p_2	p_3	p_4
-0.00016	-0.00011	-0.0086	0.25	0.0052
q	q_1	q_2	q_3	q_4
-0.0032	0.021	-0.013	0.14	1.0

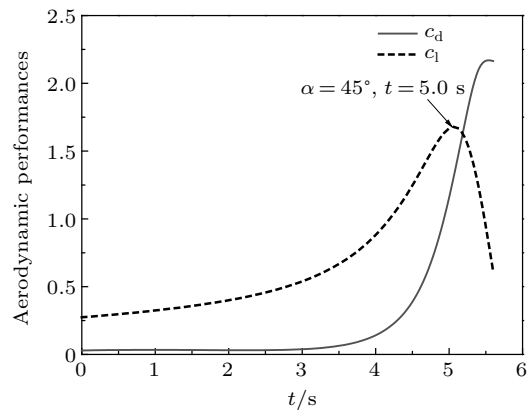


Fig. 16. Comparison of predicted drag coefficient c_d and lift coefficient c_l .

The corresponding velocity were obtained by taking the derivative of these two equations. All the fitted displacements and fitted velocities agree well with the experimental data. The predicted drag coefficient c_d and lift coefficient c_l were compared in Fig. 16 during perching. At $t = 5.0$ s, the maximum

c_1 was achieved to be 1.64, which is the value of A in Eq. (14). The effect angle of attack was estimated to be 45° at this time, while the maximum drag coefficient was achieved at the end of perching. It is interesting to find that a flat curve-segment appears in the fitted $g(x)$ between 2.0 s and 4.0 s, which implies that large lifts were generated to balance the gravity, which was irrefutably proved by the pitch-up motion of wings in Fig. 14. However, as the velocity decreased, generated lift was insufficient to hold the weight, and the eagle fell rapidly thereafter. This flap curve-segment has cushioned the direct impact to the ground

$$f(x) = p_4x^4 + p_3x^3 + p_2x^2 + p_1x + p_0, \quad (17)$$

$$g(x) = q_4x^4 + q_3x^3 + q_2x^2 + q_1x + q_0. \quad (18)$$

As the displacement, the predicted L_x deviates from the experimental one gradually with time. A deviation was observed since 2.0 s and a maximum value of 1.08 was finally achieved, which was proved by the deviation of V_x before 3.0. These velocity deviations were accumulated in the displacement responses. On the other hand, the predicted L_y fits well with the experimental one before 3.5 s, similarly the deviation in-

creased gradually until the end. It should be noted that unsteady performances of the eagle during perching is not discussed in the present study because the morphing of wings and tail was found to be accomplished in a long time with 5.6 s. It is reasonable for a quasi-steady flying estimated. To detailedly describe these unsteady performances, CFD based simulations can be an alternative method.^[42–44]

6.5. Morphing shape reconstructions

The eagle shapes were reproduced with the construction method discussed in the present study.^[45] At the initial time, a small twist angle of wing and a small pitch angle of tail were observed. On the contrary, both the extending angles of tail feathers and the first primary feathers were obtained to be extremely large. As a result, ω_2 and β were set as 7° and 3° , while α and φ_3 were set as 50° and 10° , respectively. The constructed shape was compared with the corresponding photograph as shown in Fig. 17, and a good similarity was expected. At $t = 2.0$ s, a larger twist angle of wing and a larger pitch angle of tail were observed; ω_2 , β and α were increased to 16° , 5° and 60° , respectively.

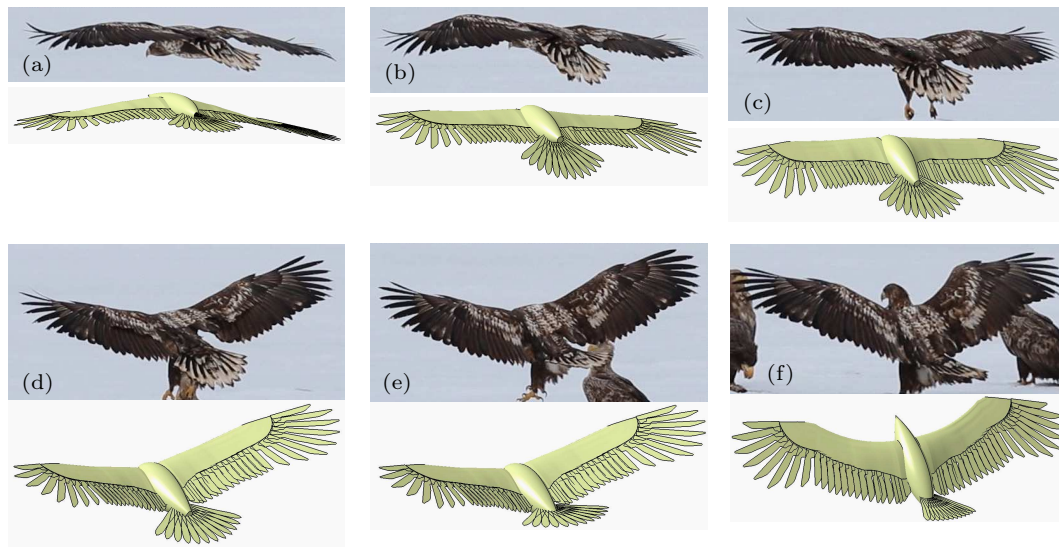


Fig. 17. Comparison of eagle photographs and the reconstructed shapes during perching: (a) 0.0 s, (b) 2.0 s, (c) 3.0 s, (d) 4.0 s, (e) 4:48 s, (f) 5:36 s.

On the other hand, the extending angle of the first primary feathers remained almost the same. At $t = 3.0$ s, ω_2 and β were estimated to increase to 18° and 8° , respectively. With a larger twist angle of wing, a larger pitching moment was estimated. Therefore, the eagle was raised up to achieve a better brace position for landing. At time 4.0 s, the eagle tried its best to stretch both the wing and tail straight to increase drags as much as possible. Also, the pitch angle of the body was adjusted to undergo deep stall. It is interesting to find that a large anhedral angle of the wing was observed, and an anhedral angle with 20° was used to reconstruct the eagle shape. At 4.8 s, the tail stuck up to prevent striking the ground, and a β angle

with -20° was used. At 5.6 s, the eagle perched, both wing and tail began to shrink, a backswept angle with about 15° was used in wing shape construction, α and β were increased set as 30° and -40° , respectively. Above all, the constructed shapes fit well with the photographs of each frame.

7. Conclusion

The flying of perching of a *Haliaeetus Albicilla* was recorded to study the wing and tail motions. It is interesting that a *Haliaeetus Albicilla* was observed to land on the ground without running or wing flapping but with combined morphing

of wing and tail to achieve the soft landing.

To reveal the morphing sequences of the eagle, a shape reconstruction method was proposed to describe wing contours and tail contours based on the scanned surface geometry of another *Aquila Chrysaetos*. The wing and tail geometries were constructed by the extracted wing planform, chord distribution and twist distribution. Thereafter, multi-body dynamics was used to derive the kinetics equations of birds using seven-DOF wing skeleton and two-DOF tail skeleton. The *Aquila Chrysaetos* model was activated to replicate the perching. Finally, perching sequences of the eagle were extracted from the video, and perching motions were estimated and fitted with polynomials. A BFGS optimization method was established and was successfully applied to predict the perching motions. Above all, the constructed shapes fit well with the photographs of each frame with the coupled method of shape reconstruction, multi-body dynamics and BFGS optimization.

Based on the observations in the present study, the rapid pitch-up motions of the wing were found to cushion the direct impact to the ground, which is different from the man-made aircrafts. It is an irrefutable proof that the key to the high manoeuvrability in bird flight lies not in the high lift-drag ratio or high lift performances, but in the way in which the wing morph to change the flying situations. Moreover, state of art of the multi-body model with more than 18 DOF of an eagle, as well as the vortex interactions of wings and tail, are considered to be the most important in morphing flies. More attention should be paid to these issues in the future research. Above all, it can be expected that the present results are a good suggestion for aerodynamics learning of birds and the next-generation unmanned aerial vehicle design.

Acknowledgments

The authors would like to thank the referees for their good and valuable suggestions which improved this paper greatly, thank the team of Zhongyong Fan for their contributions to the specimen and the 3D scanning.

References

- [1] Thomas W and Robert K 2015 *Exp. Fluids* **56** 1
- [2] Doekle G S 2014 *Mater. Today: Proc.* **1** 109
- [3] Schieber G, Born L, Bergmann P, Körner A, Mader A, Saffarian S, Betz O, Milwich M, Gresser G T and Knippers J 2018 *Bioinspiration Biomimetics* **13** 016012
- [4] Shen C and Sun M 2018 *Bioinspiration Biomimetics* **13** 016004
- [5] Buoso S, Dickinson B T and Palacios R 2018 *Bioinspiration Biomimetics* **13** 016013
- [6] Brown R H J 1953 *J. Exp. Biol.* **30** 90
- [7] Hedrick T L, Tobalske B W and Biewener A A 2002 *J. Exp. Biol.* **205** 1389
- [8] Tobalske B W, Olson N E and Dial K P 1997 *J. Exp. Zool.* **279** 313
- [9] Xuan Q, Chen Z Z, Liu Y, Huang H M, Bao G J and Zhang D 2019 *IEEE Trans. Ind. Electron.* **66** 8244
- [10] Pan Y, Ji S, Tan D and Cao H 2019 *Int. J. Adv. Manuf. Technol.* (in press)
- [11] Norberg U M 1990 *Vertebrate Flight: Mechanics, Physiology, Morphology, Ecology and Evolution* (Berlin: Springer-Verlag)
- [12] Tang D, Bao S Y, Xu M, Luo L J, Lv B B, Yu L and Cui H 2019 *Ann. Nucl. Energy* **124** 198
- [13] Tang D, Bao S Y, Luo L J, Zhu H and Cui H 2019 *Ann. Nucl. Energy* **130** 347
- [14] Yen V and Nagurka M L 1987 *Biomechanics Normal Prosthetic Gait* (1987, ASME winter Annual meeting) pp. 17–22
- [15] Ren L, Jones R K and Howard D 2007 *J. Biomechanics* **40** 1567
- [16] Parslew B and Crowther W J 2010 *J. Biomechanics* **43** 3191
- [17] Liu T S 2006 *AIAA J.* **44** 954
- [18] Andrea W, Benedikt R, Stephan K, Michael K and Wolfgang S 2014 *J. Bionic Eng.* **11** 423
- [19] Brown R E and Cogley A C 1996 *J. Exp. Zool. Part. A* **276** 112
- [20] Tang D, Liu D W and Fan Z Y 2019 *J. Test. Eval.* (in press)
- [21] Qu H and Liu X M 2019 *J. Eng. Therm.* **40** 1793 (in Chinese)
- [22] Carruthers A C, Thomas A L R, Walker S M and Taylor G K 2010 *Aeronautical J.* **114** 673
- [23] Carruthers A C, Thomas A L R and Taylor G K 2007 *J. Exp. Biol.* **210** 4136
- [24] Carruthers A C, Walker S W, Thomas A L R and Taylor G K 2010 *Proc. IME. G. J. Aero. Eng.* **224** 855
- [25] Tang D, Fan Z Y, Lei M X, Lv B B, Yu L and Cui H 2019 *Chin. Phys. B* **28** 034702
- [26] Brown R and Ferguson J 1987 *Tracks and Signs of the Birds of Britain and Europe* (Bromley: Christopher Helm)
- [27] Jones M P, Pierce K E J and Ward D 2007 *J. Exotic Pet Med.* **16** 69
- [28] John J V 2006 *Avian Flight* (Oxford: Oxford University Press)
- [29] Zinkovsky A V, Shalaha V A and Ivanov A A 1996 *Mathematical Modelling and Computer Simulation of Biomechanical Systems* (Singapore: World Scientific) p. 216
- [30] Novitskaya E, Ruestes C J, Porter M M, Lubarda V A, Meyers M A and McKittrick J 2017 *J. Mech. Behav. Biomed. Mater.* **76** 85
- [31] Tobalske B W and Dial K 1996 *J. Exp. Biol.* **199** 263
- [32] Vazquez R J 1992 *J. Morphol.* **211** 259
- [33] Vazquez R J 1994 *Zoomorphology* **114** 59
- [34] Tang D, Bao S Y, Luo L J, Mao J F, Lv B B and Guo H T 2017 *Energy* **141** 2300
- [35] Linehan T and Mohseni K 2019 *Aerosp. Sci. Technol.* **87** 73
- [36] Lv B B, Lu Z L, Guo T Q, Tang D, Yu L and Guo H T 2019 *Aerosp. Sci. Technol.* **86** 430
- [37] Usherwood J R 2009 *Exp. Fluids* **46** 991
- [38] Matthew P H, Scott W, John F F, Hans M and Richard O P 2005 *Proc. Natl. Acad. Sci. USA* **102** 11734
- [39] Chen H W, Rao F G, Shang X P, Zhang D Y and Hagiwara I 2013 *J. Bionic Eng.* **10** 341
- [40] Cornelia A, James E and Hubbard J 2018 *Modern Flexible Multi-Body Dynamics Modeling Methodology for Flapping Wing Vehicles* (New York: Academic Press) p 109
- [41] Tang D, Zhu H, Yuan W, Fan Z Y and Lei M X 2019 *Chin. Phys. B* **28** 074703
- [42] Chao L M, Pan G and Zhang D 2018 *Chin. Phys. B* **27** 114701
- [43] Li L, Qi H, Yin Z, Li D, Zhu Z, Tangwarodomnukun V and Tan D 2019 *Powder. Technol.* (in press)
- [44] Zhang X P and Zhao Q 2014 *Chin. Phys. B* **23** 064703
- [45] Proctor N and Lynch P 1998 *Manual of Ornithology* (New Haven: Yale University Press)